A Role for Barotropic Eddy–Mean Flow Feedbacks in the Zonal Wind Response to Sea Ice Loss and Arctic Amplification

BRYN RONALDS AND ELIZABETH A. BARNES

Colorado State University, Fort Collins, Colorado

(Manuscript received 25 February 2019, in final form 30 July 2019)

ABSTRACT

Previous studies have suggested that, in the zonal mean, the climatological Northern Hemisphere wintertime eddy-driven jet streams will weaken and shift equatorward in response to Arctic amplification and sea ice loss. However, multiple studies have also pointed out that this response has strong regional differences across the two ocean basins, with the North Atlantic jet stream generally weakening across models and the North Pacific jet stream showing signs of strengthening. Based on the zonal wind response with a fully coupled model, this work sets up two case studies using a barotropic model to test a dynamical mechanism that can explain the differences in zonal wind response in the North Pacific versus the North Atlantic. Results indicate that the differences between the two basins are due, at least in part, to differences in the proximity of the jet streams to the sea ice loss, and that in both cases the eddies act to increase the jet speed via changes in wave breaking location and frequency. Thus, while baroclinic arguments may account for an initial reduction in the midlatitude winds through thermal wind balance, eddy–mean flow feedbacks are likely instrumental in determining the final total response and actually act to strengthen the eddy-driven jet stream.

1. Introduction

A great deal of contemporary research looking at the midlatitude circulation has focused on how the eddy-driven jet stream will respond to external forcing associated with climate change (e.g., Peings et al. 2017; Iqbal et al. 2018; Peings et al. 2018; Ronalds et al. 2018; Screen et al. 2018a,b; Whittleston et al. 2018). One of the prominent signals of climate change is the amplified warming in the Arctic, approximately twice the globally averaged warming rate (e.g., Holland and Bitz 2003; Serreze and Francis 2006; Screen and Simmonds 2010). This phenomenon, commonly referred to as Arctic amplification, has implications for Northern Hemisphere extreme weather events, in addition to ecological and economic repercussions (e.g., Meier et al. 2014; Overland and Wang 2018; Cohen et al. 2018; Kretschmer et al. 2018; Zhang et al. 2018). It has been proposed that Arctic amplification will both directly and remotely affect the eddy-driven jet stream (e.g., Peings and Magnusdottir 2014; Hoskins and Woollings 2015; Petrie et al. 2015; Peings 2018; Screen et al. 2018b; Ronalds et al. 2018), a large-scale circulation phenomenon that steers the storm tracks (e.g., Hoskins and Valdes 1990). However, studies attempting to diagnose these impacts have widely varying results across models (as shown in Screen et al. 2018b), and also strong regional and seasonal differences (e.g., McGraw and Barnes 2016; Barnes and Simpson 2017; Ronalds et al. 2018), with recent studies finding that the largest circulation response occurs in late winter (e.g., Zappa et al. 2018). Furthermore, studies using reanalysis data struggle with causally linking the observed changes in the Arctic to any trends in the midlatitude circulation response because of the inherent noisiness of the climate system and the brevity of the climate record (e.g., Manney and Hegglin 2018; Gu et al. 2018). Due to these complications, and the large internal variability of the system, there remains a lack of dynamical understanding of the exact mechanisms linking Arctic change directly to a midlatitude response (e.g., Hoskins and Woollings 2015; Shepherd 2016; Cohen et al. 2018).

The majority of studies looking at the Arctic's ability to impact the midlatitude circulation use models of varying complexity, and diagnose changes in the large-scale zonal wind field in response to imposed sea ice loss or low-level warming (e.g., Magnusdottir et al. 2004; Deser et al. 2004, 2010; Screen and Simmonds 2013;

Corresponding author: Bryn Ronalds, bryn.ronalds@colostate.edu

DOI: 10.1175/JCLI-D-19-0157.1

Cohen et al. 2014; Peings and Magnusdottir 2014; Deser et al. 2015; Shepherd 2016; Screen et al. 2018b, among others). In the zonal mean, most models show the boreal winter Northern Hemisphere eddy-driven jet stream weakening in response to sea ice loss and Arctic amplification, and some show a slight equatorward shift as well (e.g., Screen et al. 2018b; Peings 2018; Zappa et al. 2018). While this appears to be true of the North Atlantic jet (e.g., Deser et al. 2010; Barnes and Simpson 2017; Ronalds et al. 2018; Sun et al. 2018; Zappa et al. 2018), a recent study found that many climate models project an increase in jet speed in the North Pacific in response to sea ice loss and Arctic amplification, with little to no shift in jet latitude (Barnes and Simpson 2017). Multiple studies have specifically investigated dynamical mechanisms that may explain why and how the circulation responds to external forcing (e.g., Vallis et al. 2004; Strong and Magnusdottir 2010; Barnes et al. 2010; Ring and Plumb 2007; Kim et al. 2014; Kretschmer et al. 2016; Gu et al. 2018; Ronalds et al. 2018). These proposed dynamical mechanisms are often based in Rossby wave dynamics and eddy–mean flow feedbacks, with changes in wave propagation, dissipation, breaking, and generation (i.e., baroclinic zones) leading to changes in the large-scale circulation (e.g., Strong and Magnusdottir 2010; Barnes et al. 2010; Schubert et al. 2011; Coumou et al. 2014; Kim et al. 2014; Wu and Smith 2016; Ronalds et al. 2018). For example, Kim et al. (2014) found that the Arctic warming signal in specific regions causes an enhancement of vertically propagating waves, thus leading to a weakened stratospheric polar vortex, which then feeds back onto the tropospheric circulation. Other studies have examined the impact of horizontally propagating Rossby waves, where changes in jet latitude and horizontal wind shear can cause Rossby waves to reflect rather than break (e.g., Strong and Magnusdottir 2010; Barnes et al. 2010), or vice versa.

Understanding and applying these mechanisms directly to the observations, reanalyses or model simulations remains difficult, as it is hard to separate out cause and effect from the background noise (e.g., Cohen et al. 2014; Hoskins and Woollings 2015; Samarasinghe et al. 2018). A common approach to isolating and studying specific mechanisms is using idealized models (e.g., Vallis et al. 2004; Ring and Plumb 2007; Barnes et al. 2010; Ronalds et al. 2018). This is especially useful when studying Rossby wave dynamics, which can be well represented in a simple barotropic model setup, as demonstrated by Vallis et al. (2004). It is well appreciated that Rossby wave dynamics and their resulting feedbacks with the mean flow are foundational to large-scale dynamics and will be at play in the fully coupled climate system (e.g., Strong and Magnusdottir 2010; Vallis 2017). Thus, this work, while inspired by results from a sea ice loss experiment in a fully coupled model, is focused on studying an essential, barotropic mechanism: the response of the zonal-mean flow driven by changes in eddy propagation and breaking in response to changes in the meridional wind shear. The proposed mechanism is supported by the work of Strong and Magnusdottir (2010), where they showed that changes in Rossby wave breaking bridge the gap between the initial, local, baroclinic zonal wind response to a sea ice anomaly and the longer time scale, hemisphere-wide, equivalent barotropic zonal wind response. In their study, the impact of Rossby wave breaking changes on the mean zonal wind field was estimated to account for approximately 80% of the zonally averaged zonal wind response in a fully coupled model, supporting the theory that these eddy–mean flow feedbacks are critical in understanding the real-world, midlatitude, large-scale circulation response to climate forcing.

We propose that sea ice loss and Arctic amplification directly affects the local mean flow through weakening of the surface temperature gradient, resulting in localized anomalous, low-level easterlies at high latitudes (Strong and Magnusdottir 2010). We are interested in how the eddies then respond to the initial zonal wind response, driving future changes in the large-scale circulation. Here, we explicitly represent the direct effect of the sea ice loss on the zonal flow and study the eddy response using a nondivergent barotropic model. Through this approach, we can explain both the climatological zonal wind response to Arctic amplification in a fully coupled model, and the regional differences across the two Northern Hemisphere ocean basins. Since the proposed mechanism is barotropic in nature, its effects would be present in all models and observations, though this work does not specifically address its relative importance or magnitude in the fully coupled system.

2. Model data

a. *CCSM4*

We are interested in how the zonal winds respond to sea ice loss. To motivate our idealized model experiments, we analyze sea ice loss simulations with a fully coupled global climate model, the Community Climate System Model, version 4 (CCSM4; Deser et al. 2015). The model is run at a horizontal resolution of 0.90° latitude and 1.25° longitude, with 26 vertical levels, and a full oceanic component. Full details of the experiment can be found in Deser et al. (2015), and a brief overview is also provided in Ronalds et al. (2018). We use 260 years of monthly data for both a control simulation (CONTROL), with sea ice concentration based on an

ensemble mean of six historical CCSM4 runs over the period 1980–99, and an experiment simulation (LOWICE), with sea ice concentration based on an ensemble mean of six RCP8.5 CCSM4 runs over the period 2080–99. The model uses a ghost radiative flux felt only by the ice model component to melt the sea ice to the respective ensemble mean concentrations. The variable analyzed is monthly 700 hPa zonal winds.

b. Barotropic model

As in Ronalds et al. (2018), we utilize a nondivergent barotropic model in order to begin understanding the mechanisms at play in the remote wind response to sea ice loss. We use an initial model setup identical to that of Vallis et al. (2004), where the nondivergent vorticity equation is integrated on the sphere:

$$\frac{\partial \zeta}{\partial t} + J(\psi, \zeta + f) = S - r\zeta + \kappa\nabla^4\zeta. \quad (1)$$

The left-hand side of (1) represents the Lagrangian change in absolute vorticity (relative vorticity ζ plus planetary vorticity f). The right-hand side consists of a parameterized representation of the baroclinic eddies that stir the barotropic flow, S. The amplitude of S is randomly chosen in a given range, here $[-12, 12] \times 10^{-11}$. There is also a damping parameter r and a diffusion term κ. Values for r and κ are identical to those used in Barnes et al. (2010).

Baroclinic instability in the model is represented by the imposed stochastic stirring S, generating waves within the total wavenumber range of n = 8–12. Therefore, larger waves are not specifically forced by the stirring (see Vallis et al. 2004, for more details). To simulate a meridionally confined jet we then impose a Gaussian spatial mask, damping the parameterized stirring away from a chosen latitude ϕ_s with a specified width σ_s (e.g., Vallis et al. 2004). For all experiments here we set $\sigma_s = 12°$ and vary ϕ_s. We use a resolution of T42 and a time step of 1800 s. Each simulation is run for 32 100 days, with the first 100 days discarded for spun up.

As the Arctic warms, the sea ice melts and the surface temperature gradient is weakened in the region of sea ice loss. The winds must respond to the decreased temperature gradient, and we expect them to initially locally weaken in keeping with thermal wind balance arguments. We interpret this initial weakening of the zonal winds as the direct effect of sea ice loss and the associated weakening of the temperature gradient (e.g., Strong and Magnusdottir 2010). We explicitly represent this initial impact as a meridionally constrained easterly torque acting on the zonal wind field (i.e., Ronalds et al. 2018). From there, we analyze the subsequent eddy response to the locally weakened winds. The easterly torque is a Gaussian in latitude with an amplitude of $-2.0\,\mathrm{m\,s^{-1}\,day^{-1}}$ and a standard deviation of $\sigma_f = 8°$ latitude (see also Ronalds et al. 2018). The Gaussian forcing is centered at latitude ϕ_f, which we adjust depending on the experimental setup. We run the model three times for each setup. The first run has no torque, and only the stirring, which gives us a control jet, and is referred to as NoTRQ. The second run has both stirring and torque turned on in the model, and gives us a jet resulting from the imposed torque plus any feedbacks associated with eddies reacting to the torque. We refer to this run as TOTAL. Finally, we run the model with the stirring turned off, and only the torque acting on the wind field at every time step. This results in a zonally symmetric wind field directly produced by the torque. We then add this wind field to the NoTRQ jet, giving us a resulting wind field that is the direct response of the zonal flow to the imposed torque, in the absence of eddy feedbacks. We call this run NoEDDIES, and it allows us to separate between the direct response of the zonal wind and the evolution of the wind field when eddy–mean flow feedbacks are present (TOTAL).

3. Rossby wave analysis

In the barotropic model, changes in the mean wind field driven by the imposed forcing are a combination of 1) a direct response to the forcing and 2) eddy–mean flow feedbacks resulting from changes in Rossby wave propagation and breaking/dissipation. We separate out the direct effect using the NoEDDIES simulation, and the difference between NoEDDIES and TOTAL gives us the impact of the eddies. The eddy contribution to the response is primarily controlled by changes in the convergence of eddy momentum fluxes, as well as damping and diffusion effects responding to the mean flow changes caused by the eddies. In our setup, any changes in the convergence of eddy momentum flux implies changes in wave breaking locations and/or frequencies of the eddies. We diagnose changes in wave breaking in the barotropic model using refractive indices and an algorithm to count wave breaking events, the details of which are given below.

a. Critical and reflective profiles

Rossby wave breaking theory states that waves propagating out of the jet core will be forced to break as their phase speed approaches the background zonal-mean zonal wind (e.g., Hoskins and Karoly 1981; Strong and Magnusdottir 2010). The latitude at which this occurs is referred to as the critical latitude, and it can be found using the climatological zonal-mean zonal wind

profile. This profile sets the critical latitudes for waves of all zonal wavenumbers as a function of phase speed. While in reality Rossby waves can break anywhere between the source and the critical latitudes, they favor the critical latitudes defined by the climatological jet profiles, as demonstrated in Barnes and Hartmann (2012). Depending on the gradient of absolute vorticity through which the wave is traveling (a function of both the background zonal wind and latitude), a wave may be forced to turn before it can break, generally on the poleward flank of the jet. To calculate these regions of turning, called the reflective latitudes, we use the refractive index (K^*), for example, Hoskins and Karoly (1981):

$$K^* = \cos(\phi)\sqrt{\frac{\hat{\beta}}{\overline{u}-c}}, \quad \text{and} \quad K^{*2} = k^2 + l^2, \qquad (2)$$

where k and l are the zonal and meridional wavenumbers, respectively, $\hat{\beta}$ is the meridional gradient of absolute vorticity, $\overline{u}$ is the zonal-mean zonal wind, and c is the phase speed (Hoskins and Karoly 1981; Barnes et al. 2010). The additional factor of $\cos(\phi)$ accounts for the fact that the specific wavelength associated with a zonal wavenumber k decreases with latitude (Barnes and Hartmann 2012). The waves will reflect when their zonal wavenumber is equal to K^* (i.e., $l = 0$). We can therefore rearrange (2) to give the phase speed as a function of zonal wavenumber k for when a wave reaches its turning latitude:

$$c = \overline{u} - \cos(\phi)\frac{\hat{\beta}}{k^2}. \qquad (3)$$

Equation (3) allows us to map out where waves of different sizes will be forced to turn (reflective latitude) and compare to where they prefer to break (critical latitude). The $\hat{\beta}$ term in (3) represents a dependence of the reflective profiles on both the latitude and meridional wind shear of the climatological jet profile. By analyzing the changes in reflective and critical profiles in NoEDDIES versus NoTRQ, we can evaluate exactly how the imposed torque directly affects where waves are breaking or turning. Any changes in TOTAL relative to NoEDDIES represent further adjustments by the eddies.

Since K^* depends on phase speed and the reflective profiles depend on wavenumber, we must determine the most important combinations of the two. To do so, we calculate the power spectra of the eddy momentum fluxes in both the NoTRQ and TOTAL runs as a function of both phase speed and zonal wavenumber. The space–time spectral analysis is conducted using a chunk length of 256 days, with a Hamming window and an overlap of half the chunk size. The structure of the resulting average power spectra allows us to determine which specific waves are crucial for the eddy–mean flow interactions. Further, an analysis of the difference in power between TOTAL and NoTRQ shows how the induced torque and resulting eddy feedbacks actually change which waves contribute the most to the overall eddy momentum fluxes.

b. Wave breaking counts

While the use of the refractive index has been shown to be highly accurate in predicting *where* wave breaking will occur in a climatological sense (Barnes and Hartmann 2012), it does not provide the frequency of wave breaking. There are many existing algorithms that attempt to identify and categorize wave breaking events. For the purposes of this work, we utilize the algorithm of Barnes and Hartmann (2012, see their section 2.3), using the daily output wind field data from each barotropic model experiment (NoTRQ and TOTAL from two experimental setups). To define a wave breaking event, the algorithm follows a contour of absolute vorticity and identifies a location where a meridian intersects the contour at least three times, called the overturning points (Barnes and Hartmann 2012, see their Fig. 2). These daily overturning point locations are then grouped into events of varying size, location and duration. We define the location of mixing as the centroid of the overturning points. Note that this algorithm, similarly to others, identifies all wave breaking events as those that are in the process of overturning, and assumes that each event irreversibly mixes (fully breaks), which may not always be the case. This caveat is often considered to be negligible (e.g., Barnes and Hartmann 2012; Garfinkel and Waugh 2014), though further work quantifying this assumption is needed.

4. Results

Our interest here is of the role of the eddies in determining the zonal wind response to changes in surface temperature gradients caused by Arctic amplification and sea ice loss. To motivate our idealized experiments, we begin our analysis with the sea ice loss experiment conducted using the CCSM4 (Deser et al. 2015) composed of LOWICE and CONTROL. Specifically, we examine the change in the late boreal winter Northern Hemisphere ocean basin eddy-driven jet streams, as this is the season with the largest expected large-scale atmospheric circulation response (Zappa et al. 2018). Using the January–March (JFM) 700 hPa zonal wind field we define two regions of interest, where the largest changes in zonal wind occur. The two regions are

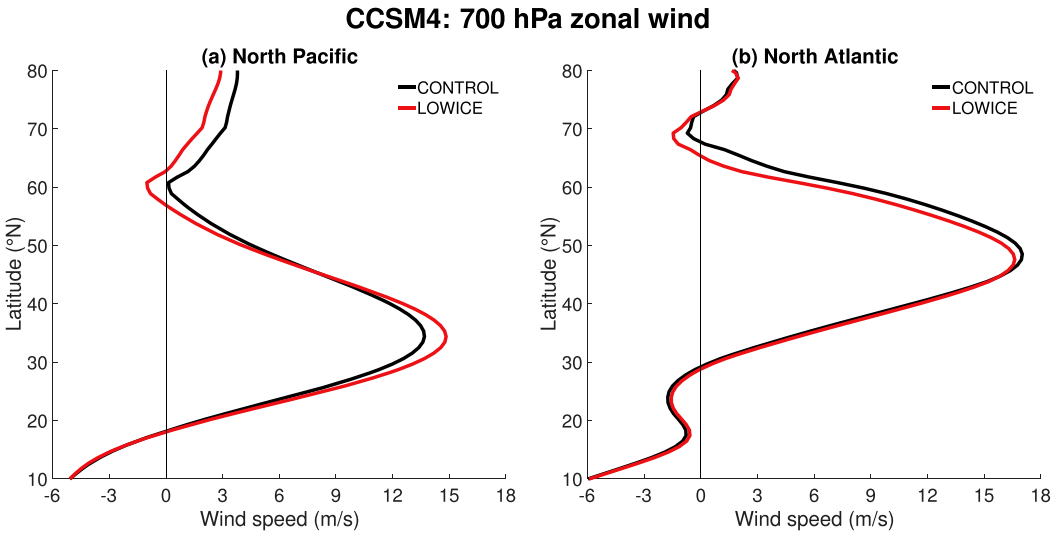

FIG. 1. Zonal-mean zonal wind profiles at 700 hPa for (a) the North Pacific and (b) the North Atlantic downstream jet regions. The control experiment, CONTROL, is in black and the sea ice loss experiment, LOWICE, is in red.

defined as the North Pacific downstream jet region (180°–225°E), and the North Atlantic downstream jet region (310°–355°E). The sector-averaged 700 hPa zonal winds across these two regions are plotted in Fig. 1, with CONTROL in black, and LOWICE in red.

The dominant change in the zonal-mean zonal flow in both the North Pacific (Fig. 1a) and the North Atlantic (Fig. 1b) is the easterly anomalies on the poleward flank of the jet. Both basins exhibit a region of enhanced easterlies and weakened westerlies poleward of the jet core in LOWICE (red) versus CONTROL (black). For both cases, the weakening of the winds is limited to north of 45°N. In the North Atlantic, this means the decreased zonal-mean zonal wind speeds extend into the jet core, both weakening the jet and asymmetrically narrowing it. This narrowing also causes a very small equatorward shift of the jet latitude of 0.7°. There are no changes to the winds south of 45°N in the North Atlantic case. Conversely, the North Pacific basin exhibits strengthened wind speeds south of 45°N, with the anomalous easterlies limited to the poleward flank of the jet. The changes in both basins' zonal-mean jet speeds and locations are considered significant at a 95% confidence level, according to a Student's t test.

The North Atlantic and North Pacific basins in the CCSM4 sea ice loss experiment have opposing responses within the jet core to sea ice loss. One possible explanation for this is that differences in jet proximity to the region of sea ice loss lead to differences in eddy–mean flow feedbacks. In the North Pacific the jet is farther south than in the North Atlantic (e.g., Hoskins and Valdes 1990), and the sea ice edge is, on average, farther north (e.g., Bitz et al. 2005), implying that the North Pacific jet is much farther from where the sea ice loss is occurring than the North Atlantic jet. We use the barotropic model to test the theory that these differences in jet latitude and distance from the region of sea ice loss drive differing eddy–mean flow feedback responses.

Barotropic model

The CCSM4 results show two regions with very different changes to the overall jet structure resulting from sea ice loss and the associated Arctic warming. From these two cases, we build an idealized model setup to explore the role of eddies in these different regional responses. The experiments use a meridionally confined stirring region to simulate the midlatitude baroclinic zone and thus drive a jet stream, and an easterly torque on the poleward flank of the jet to represent the initial circulation response to sea ice loss (see section 2 for more details). The choice of where to place the stirring and the torque are inspired by the two CCSM4 cases: the North Pacific experiment (NPAC) has the stirring placed at $\phi_s = 30°$N and the torque at $\phi_f = 70°$N, while the North Atlantic experiment (NATL) has $\phi_s = 45°$N and $\phi_f = 60°$N. The results shown here are those with the largest magnitude and those that clearly demonstrate the mechanisms involved, although the results are considered robust across ϕ_s, $\phi_f \pm 5°$, and the conclusions are consistent across all midlatitude stirring latitudes with $\phi_s > \phi_s$ (not shown). The zonal-mean zonal wind profiles

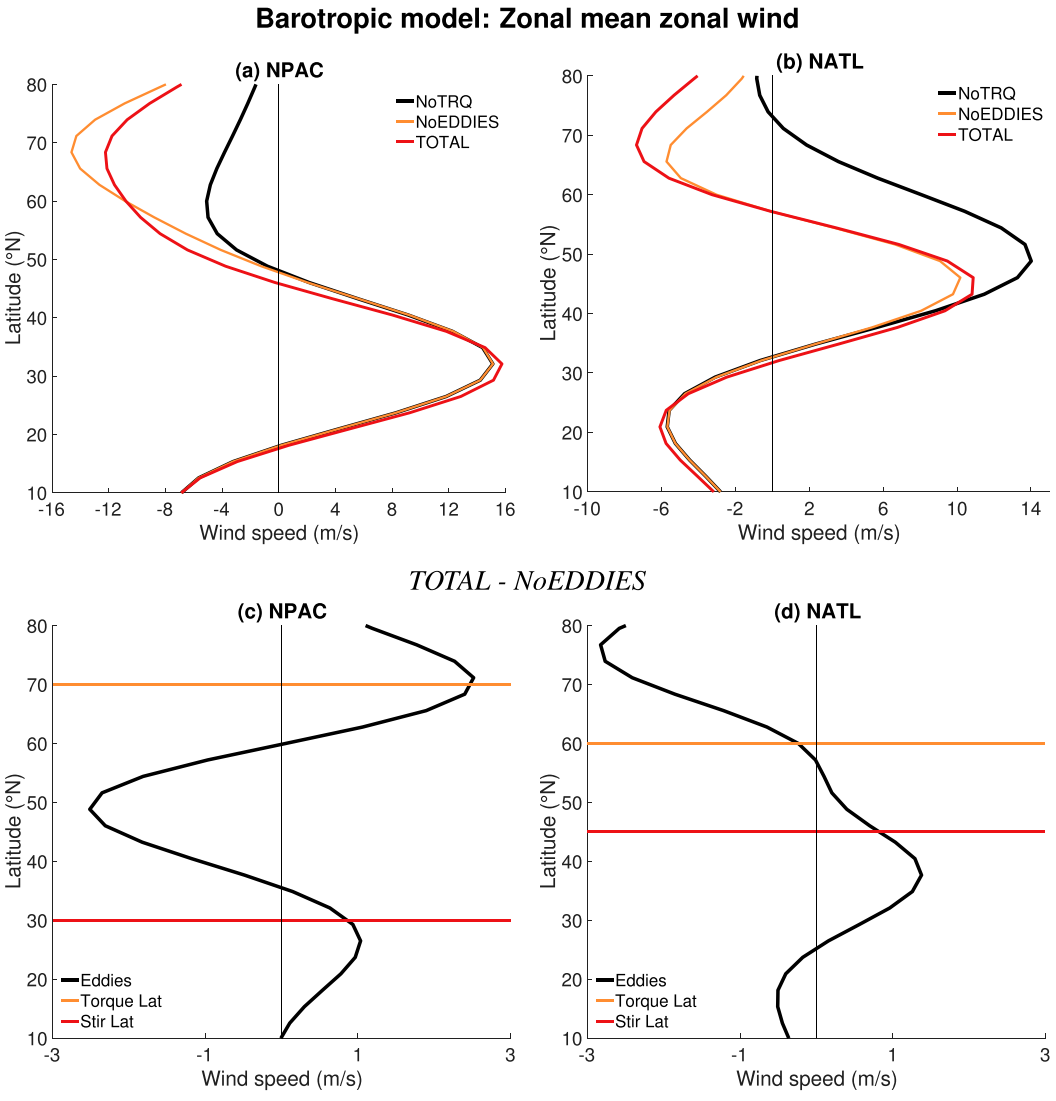

FIG. 2. (top) Zonal-mean zonal wind profiles from the (a) NPAC and (b) NATL setups. NoTRQ is in black, NoEDDIES in orange, and TOTAL is in red. (bottom) The difference in the zonal-mean zonal wind field between TOTAL and NoEDDIES in black solid for (c) NPAC and (d) NATL. The horizontal lines represent the torque and stirring latitudes (orange and red, respectively).

for the barotropic model are plotted in Fig. 2 for NPAC (Fig. 2a) and NATL (Fig. 2b). For both, the NoTRQ run is in black, NoEDDIES in orange, and TOTAL in red. The difference between TOTAL and NoEDDIES can be interpreted as the eddy contribution to the mean flow response and is plotted in Fig. 2c for NPAC and Fig. 2d for NATL. The horizontal lines in Figs. 2c and 2d represent the torque latitude (orange) and the stirring latitude (red).

The NoEDDIES (orange) response indicates the direct response of the zonal-mean zonal winds to the imposed easterly torque. The torque forces decreased wind speeds in the vicinity of the torque center, with no effect farther south (Figs. 2a and 2b, orange vs black). The NoEDDIES run in both cases exhibits a region of significantly stronger easterlies to the north of the jet compared to NoTRQ, as intended. In the NPAC case (Fig. 2a), the torque only directly affects the poleward flank, increasing the preexisting, weak easterlies. In the NATL case (Fig. 2b), the direct effect of the imposed forcing extends into the jet core, leading to strong easterlies to the north, and decreased wind speeds along the poleward flank and in the jet core.

The TOTAL (red) response represents the direct effect plus the eddy-feedback response to the imposed

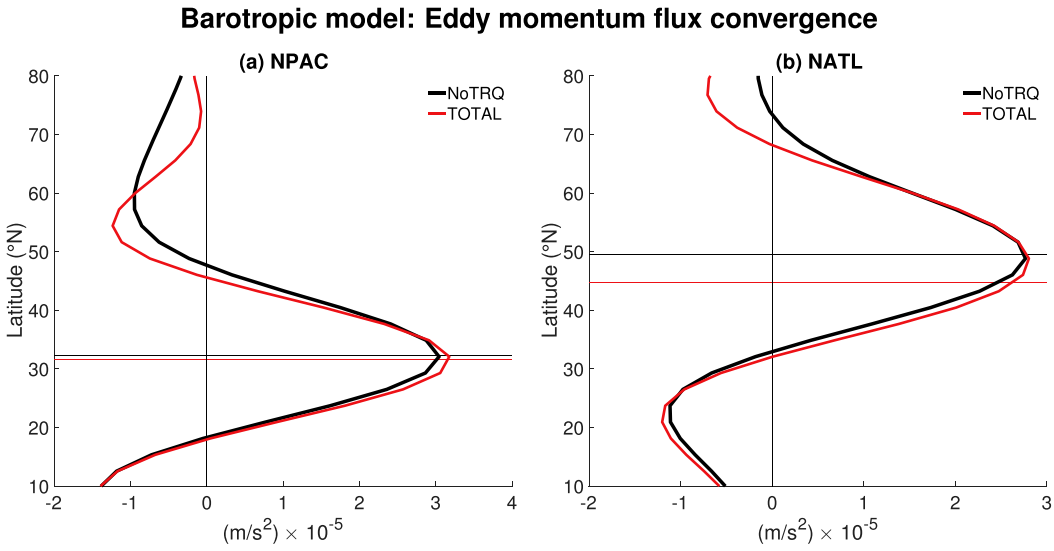

FIG. 3. The eddy momentum flux convergence (a) NPAC and (b) NATL, with NoTRQ in black and TOTAL in red. The thin, horizontal lines represent the respective jet latitudes.

torque. The TOTAL zonal-mean zonal wind maximum increases in the NPAC case (Fig. 2a), and decreases in the NATL (Fig. 2b), compared to the NoTRQ run (black). This closely resembles the behavior seen in CCSM4. The NATL TOTAL wind profile shows increased wind speeds on the equatorward flank, suggesting a larger equatorward shift of the wind profile than seen in the CCSM4 North Atlantic results. Additionally, in the region of equatorward easterlies in NATL there is a decrease in wind speeds, opposite to what we saw in the North Atlantic mean from CCSM4 (Fig. 1b). However, the general behavior of both barotropic model simulations is very similar to the CCSM4 results.

Comparing TOTAL (red) to NoEDDIES (orange) instead of NoTRQ (black) in Fig. 2 gives us the eddy response to the imposed torque. If there was no eddy response the two wind profiles would look identical, however, this is not the case. To more clearly see the full role of the eddies we plot the difference between TOTAL and NoEDDIES, shown in black solid in Figs. 2c and 2d. In both setups the eddies *increase wind speeds in the jet core*, both centered on and south of the stirring location, and decrease the winds to the north. In the NPAC case the decreased wind speeds occur relatively close to the jet core, thus narrowing the jet on the poleward side. The high-latitude wind decrease in the NATL setup occurs well north of the jet, and we do not see any poleward flank narrowing of the jet caused by the eddies. However, we do see a small widening of the jet on the equatorward flank due to the eddies, with strengthened wind speeds extending south to around 25°N. Another difference between the NPAC and NATL eddy response is seen in the region of increased wind speeds in NPAC north of 65°N, which is not seen in the NATL case. The strengthening of the northerly winds in NPAC represents less intense easterlies in that region, rather than positive wind speeds, and an explanation for this will be discussed later in the text.

The eddy-induced changes in the climatological zonal-mean zonal wind field are nearly completely explained by the eddy momentum flux convergence (Fig. 3). By definition, the simulations without stirring and only the torque acting on the zonal wind have no eddy activity, and thus, comparing TOTAL (red) to NoTRQ (black) gives us the net eddy momentum flux response to the imposed torque. For both NPAC (Fig. 3a) and NATL (Fig. 3b) there is increased eddy momentum flux convergence at the jet core, and decreased convergence to the north. The latter indicates decreased wind speeds on the poleward side of the jet, while the former indicates increased jet speeds. This is consistent with our analysis from Fig. 2. The small differences between the changes to the TOTAL wind field versus NoEDDIES in Fig. 2 and the changes to the eddy momentum flux convergence in Fig. 3 are due to the damping and diffusion of the portion of the mean flow altered by the eddies via the momentum fluxes.

Figure 3 shows that the eddies respond to the imposed torque through changes in momentum fluxes. By analyzing the power spectrum of the eddy momentum fluxes as a function of both phase speed and zonal wavenumber we can determine which waves are most important for the transport of momentum. The power spectra at the mean jet latitude is calculated for the NoTRQ and

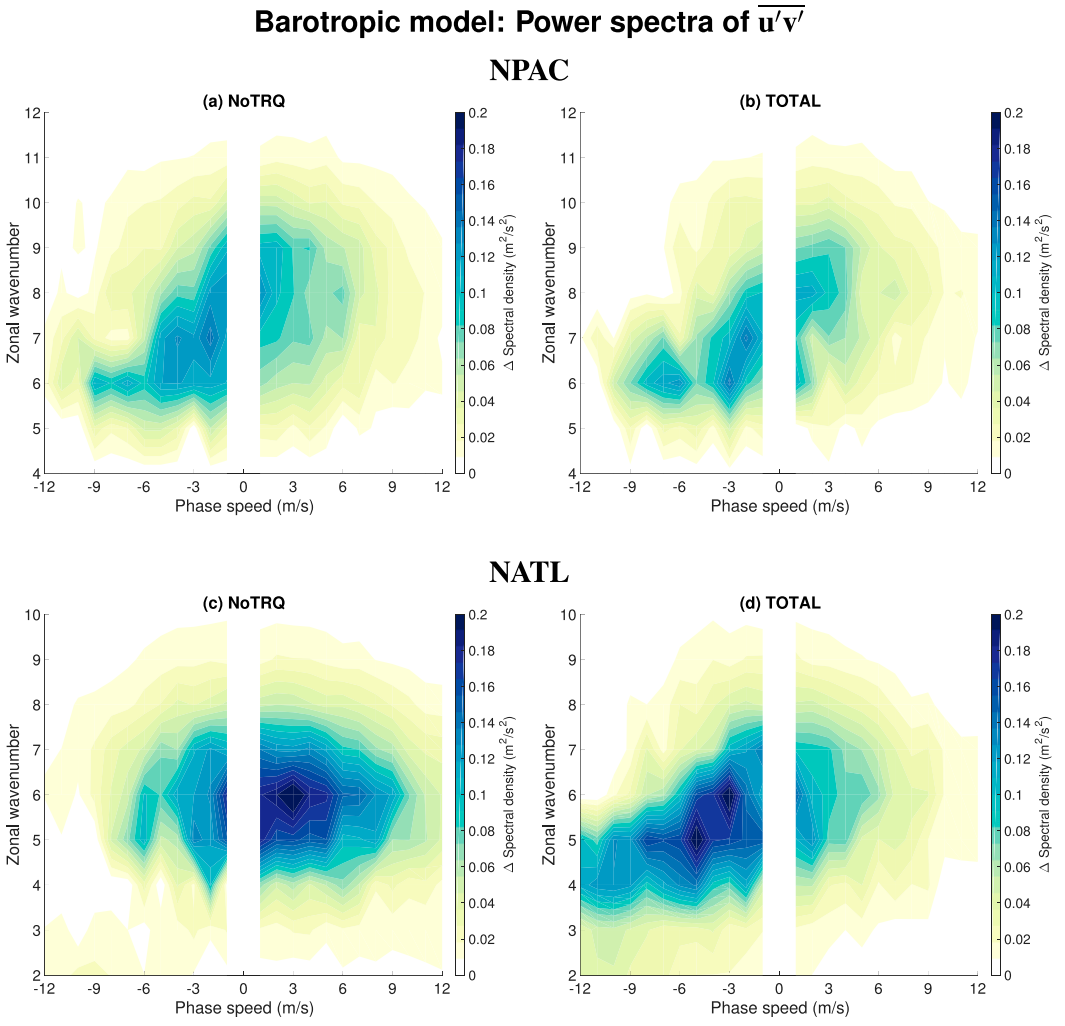

FIG. 4. The power spectra density of the eddy momentum fluxes for the NPAC (a) NoTRQ and (b) TOTAL experiments, and the NATL (c) NoTRQ and (d) TOTAL experiments. The spectra are evaluated at the respective jet latitudes, and are a function of both phase speed and wavenumber. The wavenumber range for (a),(b) NPAC is k = 4–12, and for (c),(d) NATL it is k = 2–10.

TOTAL runs from both experiments and plotted in Fig. 4. The conclusions drawn remain unchanged if we calculate the power spectra at the stirring latitudes, or calculate the average power across the stirring regions.

In the NPAC case the power spectra in NoTRQ (Fig. 4a) and TOTAL (Fig. 4b) both show peaks in power for phase speeds around -9 to $5\,\mathrm{m\,s^{-1}}$, and wavenumbers k = 5–9. The spectra is similar between TOTAL and NoTRQ, indicating that in the NPAC case the imposed torque does not change which waves are most important for fluxing momentum. In the NATL case (Figs. 4c,d), the power is generally shifted to smaller wavenumbers than in NPAC. This is due to the higher-latitude stirring in NATL, which has been previously shown to shift the power to larger wavelengths (e.g., Barnes and Hartmann 2011). For the NATL NoTRQ run (Fig. 4c) the waves primarily responsible for the flux of momentum are generally within the zonal wavenumber range of k = 4–7, peaking at k = 6, and phase speeds of $-6\,\mathrm{m\,s^{-1}}$ to about $9\,\mathrm{m\,s^{-1}}$. In the TOTAL run (Fig. 4d), however, the peak power shifts significantly, and is concentrated at negative phase speeds and slightly smaller wavenumbers. The biggest changes occur around wavenumbers k = 5–6, where there is almost no power remaining for waves with positive phase speeds in TOTAL and there is a significant increase in power at negative phase speeds. That is, the imposed torque changes which waves are most important for the transportation of easterly momentum out of the jet core. This response is similar to that seen in Strong and Magnusdottir (2010),

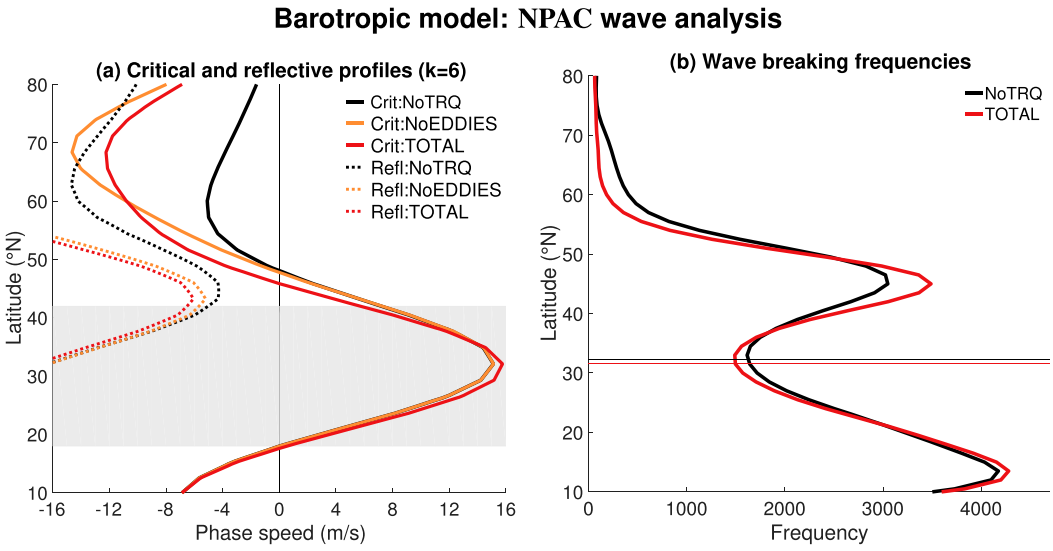

FIG. 5. (a) The NPAC critical (solid) and reflective (dotted) profiles for zonal wavenumber $k = 6$. NoTRQ is in black, NoEDDIES in orange, and TOTAL is in red. The thin, gray, horizontal lines indicate the $\phi_s \pm 1\sigma_s$ extent of the Gaussian stirring mask. (b) The NPAC wave breaking frequencies for both NoTRQ (black) and TOTAL (red). The position of maximum climatological zonal-mean zonal winds is indicated by the thin, horizontal lines.

where they observe a shift in power to smaller phase speeds and zonal wavenumber in response to imposed sea ice loss in a fully coupled climate model.

Changes in eddy momentum flux convergence in response to an imposed torque, as shown in Fig. 3, imply changes in the eddy activity, specifically changes in the propagation and breaking of waves. Similar to previous work, (e.g., Barnes and Hartmann 2012; Lorenz 2014; Ronalds et al. 2018), we use the critical and reflective profiles associated with each run to analyze changes in wave propagation and the locations of wave breaking. Figure 4 shows which waves have the most power in fluxing momentum, allowing us to objectively pick the reflective profiles of interest in both experiments, and focusing our analysis on the crucial phase speeds. We further supplement the information provided by the refractive index profiles with counts of NoTRQ and TOTAL wave breaking events for both NPAC and NATL in the sections below.

1) EDDY ACTIVITY: NORTH PACIFIC

In the NPAC case we found the reflective profile associated with $k = 6$ to be the clearest representation of the eddy response to the imposed torque. The NPAC critical (solid) and reflective (dotted) profiles for zonal wavenumber $k = 6$ are shown in Fig. 5a, with NoTRQ in black, TOTAL in red, and NoEDDIES in orange. The gray shading represents the one standard deviation extent of the Gaussian-shaped stirring mask. Remember that while there are no eddies responding to the altered zonal-mean zonal wind profile in the NoEDDIES run, we can still use its critical and reflective profiles to tell us how the eddies would respond to the torque, if they were present. Figure 5b shows the NPAC wave breaking frequencies for the NoTRQ (black) and TOTAL (red) runs, as a function of latitude. The thin, horizontal lines represent the jet latitudes from both runs.

From Figs. 2c and 3a, we know that the eddies respond to the torque and act to increase the speed of the jet via increased convergence of westerly momentum into the jet core. Furthermore, from Rossby wave arguments, this could either indicate increased wave breaking on the flanks of the jet in TOTAL relative to NoTRQ, or decreased wave breaking within the jet itself. We are therefore interested in how the imposed torque changes both the reflective and critical profiles in NoEDDIES relative to NoTRQ. Looking first at the reflective profiles (dotted curves), we note a small reduction in the NoEDDIES reflective profile relative to the NoTRQ profile (orange vs black dotted curves). There is a small range of phase speeds, between -5.2 and $-4.3\,\mathrm{m\,s^{-1}}$, where waves are reflected in NoTRQ but would be able to propagate poleward until reaching a critical latitude and breaking in NoEDDIES. Therefore, we expect there to be an increase in wave breaking on the poleward flank, and looking at Fig. 5b, we see a significant increase in wave breaking on the poleward flank, consistent with the changes to the reflective profiles. There is also a decrease in wave breaking in the jet core due to the same changes in reflective profiles. In NoTRQ the

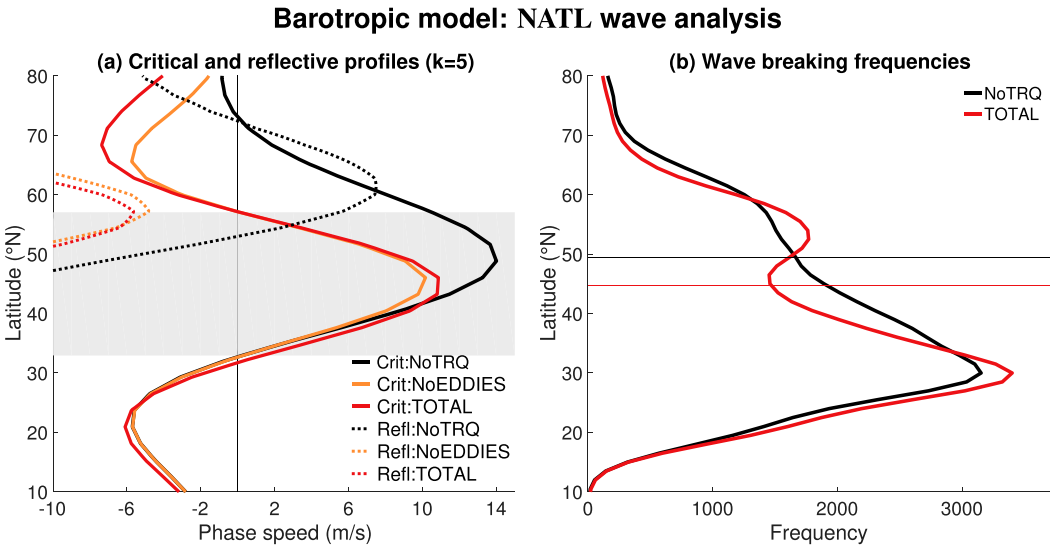

FIG. 6. (a) The NATL critical (solid) and reflective (dotted) profiles for zonal wavenumber $k = 5$. NoTRQ is in black, NoEDDIES in orange, and TOTAL is in red. The thin, gray, horizontal lines indicate the $\phi_s \pm 1\sigma_s$ extent of the Gaussian stirring mask. (b) The NATL wave breaking frequencies for both NoTRQ (black) and TOTAL (red). The position of maximum climatological zonal-mean zonal winds is indicated by the thin, horizontal lines.

reflected waves likely broke once they reentered the stirring region, whereas in TOTAL these waves instead break on the poleward jet flank. While the torque causes the initial relaxation of the reflective profile, the increased wave breaking on the poleward flank decreases the wind speeds and further alters the meridional shear of the zonal wind, relaxing the reflective profile further (red dotted), so that waves with negative phase speeds up to $-6.1\,\mathrm{m\,s^{-1}}$ are now able to break on the poleward flank of the jet. While small, this range of phase speeds exhibits a peak in power at $k = 6$ (Figs. 4a,b), and thus is considered crucial to the total eddy response.

The imposed torque also changes the critical profiles by enhancing the easterlies north of 50°N (Fig. 5a, orange vs black solid), meaning waves break at lower latitudes in TOTAL than in NoTRQ. This change results in even more wave breaking on the poleward flank, at around 45°N, and less wave breaking at higher latitudes, closer to 60°N, as seen in Fig. 5b. This decrease in wave breaking at high latitudes is the reason we see increased wind speeds there in Fig. 2c.

2) EDDY ACTIVITY: NORTH ATLANTIC

For the NATL, Figs. 4c and 4d show that the eddy momentum flux power spectra significantly changes between NoTRQ and TOTAL, and we found that wavenumber $k = 5$ most clearly demonstrates the eddy response and the reasons for the shift in power from positive to negative phase speeds. We once again focus our analysis on negative phase speeds, as this is where the power is most concentrated when the torque is imposed. As in NPAC, we plot the corresponding critical (solid) and reflective (dotted) profiles in Fig. 6a, and the wave breaking frequencies in Fig. 6b.

Looking at Fig. 6a, we note some similarities to the NPAC experiment. In both experiments, the biggest changes in reflective and critical profiles occur on the poleward flank of the jet, with enhanced critical profiles in NoEDDIES as compared to NoTRQ (orange vs black solid) and a relaxed reflective profile (orange vs black dotted). As in NPAC, a reduction in the reflective profile in NoEDDIES relative to NoTRQ means that waves propagating poleward are able to reach a critical latitude and break, rather than being turned back. This suggests increased wave breaking on the poleward flank of the jet, and decreased wave breaking within the stirring region in TOTAL relative to NoTRQ, both of which are seen in Fig. 6b. In the NATL case, however, the decreased wave breaking in the jet core in TOTAL relative to NoTRQ in Fig. 6b is much larger and more extensive than in NPAC, and there is a significant increase in wave breaking on the equatorward flank as well.

In the NATL case, the reflective profile in NoTRQ (black dotted) is so strong that many waves, especially those with negative phase speeds, are trapped and break within the stirring region. This occurs where the generation region (gray shading) is bounded by the reflective profile (black dotted curve). As a result, the NATL NoTRQ case has a great deal of wave breaking occurring within the jet core, as seen in Fig. 6b (black curve),

with no clear local minima at the jet latitude. The imposed torque narrows the jet significantly on the poleward flank, greatly increasing the meridional wind shear, resulting in a large reduction of the reflective profiles. This means that waves with negative phase speeds are no longer trapped in the generation region in TOTAL and can propagate both poleward and equatorward, resulting in increased wave breaking on both flanks of the jet, and decreased wave breaking in the stirring region itself, as evident in Fig. 6b (red curve). In addition, in TOTAL it is *only* waves with negative phase speeds that can propagate out of the stirring region before encountering a critical latitude (Fig. 6a, red curve). Only if a wave breaks outside the generation region is there a net momentum flux, further emphasizing the increased power at negative phase speeds in TOTAL relative to NoTRQ seen in Figs. 4c and 4d, and explaining the reduction in power at positive phase speeds.

Waves with negative phase speeds exhibit decreased wave breaking in the stirring region in TOTAL versus NoTRQ, and increased wave breaking outside the stirring region on both flanks of the jet. Both of these changes in wave breaking lead to increased jet speeds via the convergence of westerly momentum into the stirring region. The increased convergence of westerly momentum into the stirring region is associated with increased wave breaking on both flanks of the jet, further enhancing easterlies in these two regions (Fig. 2b red vs black). The TOTAL wave breaking frequencies now have a clear, local minima in the jet core, a distinct peak on the poleward flank of the jet and an enhanced peak on the equatorward flank (Fig. 6b, red curve). The decrease in wave breaking within the stirring region is mostly confined south of the jet latitude (thin, horizontal, red line), accounting for the increased wind speeds in that region and the slight, equatorward shift of the jet seen in TOTAL relative to NoEDDIES (Fig. 2b).

5. Discussion and conclusions

Using only a zonally symmetric barotropic model, we are able to replicate key aspects of the fully coupled CCSM4 model Northern Hemisphere ocean basin jet stream responses to sea ice loss. Specifically, in the CCSM4, the North Atlantic jet weakens and shifts slightly equatorward, while the North Pacific jet strengthens and extends eastward. The nature of the barotropic model allows us to separate the changes into the direct, forced response, and the response due to eddy feedbacks. Utilizing two experimental setups that represent the two basins, we find that in *both* cases the barotropic eddy–mean flow feedbacks are working to *increase* jet speeds, and that the *net* zonal wind response strongly depends on the jet latitude relative to the imposed forcing. In the North Pacific setup the jet is far enough away from the forcing that the net effect is an increase in jet speed due to the eddies, and the direct response is isolated to the poleward flank. In the North Atlantic setup the jet is closer to the imposed forcing and the net effect is a decrease in jet speed due to the direct response, counteracted by the eddy response. In both cases the eddy response is the same, working to increase the jet speeds and further enhance the easterlies on the poleward flank of the jet via increases in westerly momentum convergence in the jet core. These eddy responses are driven primarily by changes to the reflective profiles, which dictate which waves are turned back and which reach a critical latitude and break. Changes to the critical profiles also affect where waves are preferentially breaking on the poleward flank, and thus, also contribute to the total eddy response.

The two simulated cases shown in this work were chosen for their similarities to the CCSM4 ocean basin jet streams. In testing the sensitivity of the barotropic model results to the placement of the stirring and torque latitudes, we found the eddy response to be consistent for all midlatitude stirring and imposed easterly torques poleward of the jet. In all cases, the eddies strengthen the westerlies in the jet core and to the south and induce a region of easterly wind anomalies on the poleward flank of the jet. The precise location of the maximum eddy impact on the mean flow depends on both the latitude of the stirring and how close it is to the torque. Both of these factors strongly influence the reflective profiles, either via planetary or relative vorticity, which, in turn, controls which waves propagate far enough from the jet to break and contribute to the net convergence of eddy momentum flux into the stirring region.

The barotropic eddy–mean flow feedbacks found in this work support the CCSM4 result of increased jet speeds in the North Pacific in response to sea ice loss, although we do not expect them to be the full story in the more complex system. As seen in the highly idealized barotropic model, the application of a strong easterly torque only results in small increases in jet speeds in the North Pacific experiment, nowhere near the increase seen in the CCSM4. However, baroclinic feedbacks between changes in wave propagation and wave generation are almost certainly at play within the coupled system and are not included in our barotropic model setup. Barnes and Thompson (2014) showed that adding a baroclinic feedback by allowing for slight shifts of the stirring region is key in determining the magnitude of the zonal wind response to forcing, with barotropic feedbacks setting the structure and sign of the response. It is also possible that there are additional feedbacks

associated with a change in the strength of the baroclinic zone in response to external forcing, which would be of interest to examine further.

The level of complexity in the CCSM4 experiment suggests that there may be many additional mechanisms at play, and the wide range of model responses to climate forcings shown in previous work mean that one model may not be considered representative of the true atmospheric circulation response (e.g., Zappa et al. 2018). However, the findings of this work and the increased understanding of the barotropic mechanisms involved highlight the role of barotropic eddy–mean flow feedbacks in driving the jet stream response to Arctic amplification and sea ice loss. Further, the same eddy–mean flow feedbacks are present in two very different experimental setups, and the results stress the importance of jet latitude in determining the net response to forcing.

Acknowledgments. The authors thank Lantao Sun for providing the CCSM4 data and the four anonymous reviewers whose comments were exceedingly helpful in improving this work. The authors are supported by the Climate and Large-Scale Dynamics Program of the National Science Foundation under Grant 1545675.

REFERENCES

Barnes, E. A., and D. L. Hartmann, 2011: Rossby wave scales, propagation, and the variability of eddy-driven jets. *J. Atmos. Sci.*, **68**, 2893–2908, https://doi.org/10.1175/JAS-D-11-039.1.

——, and ——, 2012: Detection of Rossby wave breaking and its response to shifts of the midlatitude jet with climate change. *J. Geophys. Res.*, **117**, D09117, https://doi.org/10.1029/2012JD017469.

——, and D. W. J. Thompson, 2014: Comparing the roles of barotropic versus baroclinic feedbacks in the atmosphere's response to mechanical forcing. *J. Atmos. Sci.*, **71**, 177–194, https://doi.org/10.1175/JAS-D-13-070.1.

——, and I. R. Simpson, 2017: Seasonal sensitivity of the Northern Hemisphere jet streams to Arctic temperatures on subseasonal timescales. *J. Climate*, **30**, 10 117–10 137, https://doi.org/10.1175/JCLI-D-17-0299.1.

——, D. L. Hartmann, D. M. W. Frierson, and J. Kidston, 2010: Effect of latitude on the persistence of eddy-driven jets. *Geophys. Res. Lett.*, **37**, L11804, https://doi.org/10.1029/2010GL043199.

Bitz, C. M., M. M. Holland, E. C. Hunke, and R. E. Moritz, 2005: Maintenance of the sea ice edge. *J. Climate*, **18**, 2903–2921, https://doi.org/10.1175/JCLI3428.1.

Cohen, J., and Coauthors, 2014: Recent Arctic amplification and extreme mid-latitude weather. *Nat. Geosci.*, **7**, 627–637, https://doi.org/10.1038/ngeo2234.

——, K. Pfeiffer, and J. A. Francis, 2018: Warm Arctic episodes linked with increased frequency of extreme winter weather in the United States. *Nat. Commun.*, **9**, 869, https://doi.org/10.1038/s41467-018-02992-9.

Coumou, D., V. Petoukhov, S. Rahmstorf, S. Petri, and H. J. Schellnhuber, 2014: Quasi-resonant circulation regimes and hemispheric synchronization of extreme weather in boreal summer. *Proc. Natl. Acad. Sci. USA*, **111**, 12 331–12 336, https://doi.org/10.1073/pnas.1412797111.

Deser, C., G. Magnusdottir, R. Saravanan, and A. Phillips, 2004: The effects of North Atlantic SST and sea ice anomalies on the winter circulation in CCM3. Part II: Direct and indirect components of the response. *J. Climate*, **17**, 877–889, https://doi.org/10.1175/1520-0442(2004)017<0877:TEONAS>2.0.CO;2.

——, R. Tomas, M. Alexander, and D. Lawrence, 2010: The seasonal atmospheric response to projected Arctic sea ice loss in the late twenty-first century. *J. Climate*, **23**, 333–351, https://doi.org/10.1175/2009JCLI3053.1.

——, ——, and L. Sun, 2015: The role of ocean–atmosphere coupling in the zonal-mean atmospheric response to Arctic sea ice loss. *J. Climate*, **28**, 2168–2186, https://doi.org/10.1175/JCLI-D-14-00325.1.

Garfinkel, C. I., and D. W. Waugh, 2014: Tropospheric Rossby wave breaking and variability of the latitude of the eddy-driven jet. *J. Climate*, **27**, 7069–7085, https://doi.org/10.1175/JCLI-D-14-00081.1.

Gu, S., Y. Zhang, Q. Wu, and X.-Q. Yang, 2018: The linkage between Arctic sea ice and midlatitude weather: In the perspective of energy. *J. Geophys. Res. Atmos.*, **123**, 11 536–11 550, https://doi.org/10.1029/2018JD028743.

Holland, M. M., and C. M. Bitz, 2003: Polar amplification of climate change in coupled models. *Climate Dyn.*, **21**, 221–232, https://doi.org/10.1007/s00382-003-0332-6.

Hoskins, B. J., and D. J. Karoly, 1981: The steady linear response of a spherical atmosphere to thermal and orographic forcing. *J. Atmos. Sci.*, **38**, 1179–1196, https://doi.org/10.1175/1520-0469(1981)038<1179:TSLROA>2.0.CO;2.

——, and P. J. Valdes, 1990: On the existence of storm tracks. *J. Atmos. Sci.*, **47**, 1854–1864, https://doi.org/10.1175/1520-0469(1990)047<1854:OTEOST>2.0.CO;2.

Hoskins, B., and T. Woollings, 2015: Persistent extratropical regimes and climate extremes. *Curr. Climate Change Rep.*, **1**, 115–124, https://doi.org/10.1007/s40641-015-0020-8.

Iqbal, W., W.-N. Leung, and A. Hannachi, 2018: Analysis of the variability of the North Atlantic eddy-driven jet stream in CMIP5. *Climate Dyn.*, **51**, 235–247, https://doi.org/10.1007/s00382-017-3917-1.

Kim, B. M., S. W. Son, S. K. Min, J. H. Jeong, S. J. Kim, X. Zhang, T. Shim, and J. H. Yoon, 2014: Weakening of the stratospheric polar vortex by Arctic sea-ice loss. *Nat. Commun.*, **5**, 4646, https://doi.org/10.1038/NCOMMS5646.

Kretschmer, M., D. Coumou, J. F. Donges, and J. Runge, 2016: Using causal effect networks to analyze different Arctic drivers of midlatitude winter circulation. *J. Climate*, **29**, 4069–4081, https://doi.org/10.1175/JCLI-D-15-0654.1.

——, ——, L. Agel, M. Barlow, E. Tziperman, and J. Cohen, 2018: More-persistent weak stratospheric polar vortex states linked to cold extremes. *Bull. Amer. Meteor. Soc.*, **99**, 49–60, https://doi.org/10.1175/BAMS-D-16-0259.1.

Lorenz, D. J., 2014: Understanding midlatitude jet variability and change using Rossby wave chromatography: Poleward-shifted jets in response to external forcing. *J. Atmos. Sci.*, **71**, 2370–2389, https://doi.org/10.1175/JAS-D-13-0200.1.

Magnusdottir, G., C. Deser, and R. Saravanan, 2004: The effects of North Atlantic SST and sea ice anomalies on the winter circulation in CCM3. Part I: Main features and storm track characteristics of the response. *J. Climate*, **17**, 857–876, https://doi.org/10.1175/1520-0442(2004)017<0857:TEONAS>2.0.CO;2.

Manney, G. L., and M. I. Hegglin, 2018: Seasonal and regional variations of long-term changes in upper-tropospheric jets from reanalyses. *J. Climate*, **31**, 423–448, https://doi.org/10.1175/JCLI-D-17-0303.1.

McGraw, M. C., and E. A. Barnes, 2016: Seasonal sensitivity of the eddy-driven jet to tropospheric heating in an idealized AGCM. *J. Climate*, **29**, 5223–5240, https://doi.org/10.1175/JCLI-D-15-0723.1.

Meier, W. N., and Coauthors, 2014: Arctic sea ice in transformation: A review of recent observed changes and impacts on biology and human activity. *Rev. Geophys.*, **52**, 185–217, https://doi.org/10.1002/2013RG000431.

Overland, J. E., and M. Wang, 2018: Arctic-midlatitude weather linkages in North America. *Polar Sci.*, **16**, 1–9, https://doi.org/10.1016/j.polar.2018.02.001.

Peings, Y., 2018: The atmospheric response to sea-ice loss. *Nat. Climate Change*, **8**, 664–665, https://doi.org/10.1038/s41558-018-0243-5.

——, and G. Magnusdottir, 2014: Response of the wintertime Northern Hemisphere atmospheric circulation to current and projected Arctic sea ice decline: A numerical study with CAM5. *J. Climate*, **27**, 244–264, https://doi.org/10.1175/JCLI-D-13-00272.1.

——, J. Cattiaux, S. Vavrus, G. Magnusdottir, and Y. Peings, 2017: Late twenty-first-century changes in the midlatitude atmospheric circulation in the CESM large ensemble. *J. Climate*, **30**, 5943–5960, https://doi.org/10.1175/JCLI-D-16-0340.1.

——, ——, S. J. Vavrus, and G. Magnusdottir, 2018: Projected squeezing of the wintertime North-Atlantic jet. *Environ. Res. Lett.*, **13**, 074016, https://doi.org/10.1088/1748-9326/aacc79.

Petrie, R. E., L. C. Shaffrey, and R. T. Sutton, 2015: Atmospheric impact of Arctic sea ice loss in a coupled ocean–atmosphere simulation. *J. Climate*, **28**, 9606–9622, https://doi.org/10.1175/JCLI-D-15-0316.1.

Ring, M. J., and R. A. Plumb, 2007: Forced annular mode patterns in a simple atmospheric general circulation model. *J. Atmos. Sci.*, **64**, 3611–3626, https://doi.org/10.1175/JAS4031.1.

Ronalds, B., E. Barnes, and P. Hassanzadeh, 2018: A barotropic mechanism for the response of jet stream variability to Arctic amplification and sea ice loss. *J. Climate*, **31**, 7069–7085, https://doi.org/10.1175/JCLI-D-17-0778.1.

Samarasinghe, S. M., M. C. McGraw, E. A. Barnes, and I. Ebert-Uphoff, 2018: A study of links between the Arctic and the midlatitude jet stream using Granger and Pearl causality. *Environmetrics*, **40**, e2540, https://doi.org/10.1002/ENV.2540.

Schubert, S., H. Wang, and M. Suarez, 2011: Warm season subseasonal variability and climate extremes in the Northern Hemisphere: The role of stationary Rossby waves. *J. Climate*, **24**, 4773–4792, https://doi.org/10.1175/JCLI-D-10-05035.1.

Screen, J. A., and I. Simmonds, 2010: The central role of diminishing sea ice in recent Arctic temperature amplification. *Nature*, **464**, 1334–1337, https://doi.org/10.1038/nature09051.

——, and ——, 2013: Exploring links between Arctic amplification and mid-latitude weather. *Geophys. Res. Lett.*, **40**, 959–964, https://doi.org/10.1002/grl.50174.

——, T. J. Bracegirdle, and I. Simmonds, 2018a: Polar climate change as manifest in atmospheric circulation. *Curr. Climate Change Rep.* https://doi.org/10.1007/S40641-018-0111-4.

——, and Coauthors, 2018b: Consistency and discrepancy in the atmospheric response to Arctic sea-ice loss across climate models. *Nat. Geosci.*, **11**, 155–163, https://doi.org/10.1038/s41561-018-0059-y.

Serreze, M. C., and J. A. Francis, 2006: The Arctic amplification debate. *Climatic Change*, **76**, 241–264, https://doi.org/10.1007/s10584-005-9017-y.

Shepherd, T. G., 2016: Effects of a warming Arctic. *Science*, **353**, 989–990, https://doi.org/10.1126/science.aag2349.

Strong, C., and G. Magnusdottir, 2010: The role of Rossby wave breaking in shaping the equilibrium atmospheric circulation response to North Atlantic boundary forcing. *J. Climate*, **23**, 1269–1276, https://doi.org/10.1175/2009JCLI2676.1.

Sun, L., M. Alexander, and C. Deser, 2018: Evolution of the global coupled climate response to Arctic sea ice loss during 1990–2090 and its contribution to climate change. *J. Climate*, **31**, 7823–7843, https://doi.org/10.1175/JCLI-D-18-0134.1.

Vallis, G. K., 2017: *Atmospheric and Oceanic Fluid Dynamics*. 2nd ed. Cambridge University Press, 964 pp.

——, E. P. Gerber, P. J. Kushner, and B. A. Cash, 2004: A mechanism and simple dynamical model of the North Atlantic Oscillation and annular modes. *J. Atmos. Sci.*, **61**, 264–280, https://doi.org/10.1175/1520-0469(2004)061<0264:AMASDM>2.0.CO;2.

Whittleston, D., K. A. McColl, and D. Entekhabi, 2018: Multimodel future projections of wintertime North Atlantic and North Pacific tropospheric jets: A Bayesian analysis. *J. Climate*, **31**, 2533–2545, https://doi.org/10.1175/JCLI-D-17-0316.1.

Wu, Y., and K. L. Smith, 2016: Response of Northern Hemisphere midlatitude circulation to Arctic amplification in a simple atmospheric general circulation model. *J. Climate*, **29**, 2041–2058, https://doi.org/10.1175/JCLI-D-15-0602.1.

Zappa, G., F. Pithan, and T. G. Shepherd, 2018: Multimodel evidence for an atmospheric circulation response to Arctic sea ice loss in the CMIP5 future projections. *Geophys. Res. Lett.*, **45**, 1011–1019, https://doi.org/10.1002/2017GL076096.

Zhang, X., T. Jung, M. Wang, Y. Luo, T. Semmler, and A. Orr, 2018: Preface to the special issue: Towards improving understanding and prediction of Arctic change and its linkage with Eurasian mid-latitude weather and climate. *Adv. Atmos. Sci.*, **35**, 1–4, https://doi.org/10.1007/s00376-017-7004-7.